Transition from Collisional to Collisionless Regimes in Interpenetrating Plasma Flows on the National Ignition Facility

J. S. Ross *et al.*

Transition from collisional to collisionless regimes in interpenetrating plasma flows on the National Ignition Facility

J. S. Ross,[1] D. P. Higginson,[1] D. Ryutov,[1] F. Fiuza,[2] R. Hatarik,[1] C. M. Huntington,[1] D. H. Kalantar,[1] A. Link,[1] B. B. Pollock,[1] B. A. Remington,[1] H. G. Rinderknecht,[1] G. F. Swadling,[1] D. P. Turnbull,[1] S. Weber,[1] S. Wilks,[1] D. H. Froula,[3] M. J. Rosenberg,[3] T. Morita,[4] Y. Sakawa,[5] H. Takabe,[5] R. P. Drake,[6] C. Kuranz,[6] G. Gregori,[7] J. Meinecke,[7] M. C. Levy,[7] M. Koenig,[8] A. Spitkovsky,[9] R. D. Petrasso,[10] C. K. Li,[10] H. Sio,[10] B. Lahmann,[10] A. B. Zylstra,[11] and H.-S. Park[1]

[1]*Lawrence Livermore National Laboratory, P.O. Box 808, Livermore, California 94551*
[2]*SLAC National Accelerator Laboratory, Stanford University, Stanford, CA 94305, USA.*
[3]*Laboratory for Laser Energetics, University of Rochester,*
250 E. River Road, Rochester, New York 14623
[4]*Kyushu University, 6-1 Kasuga-Koen, Kasuga, Fukuoka 816-8580, Japan*
[5]*Osaka University, 1-1 Yamadaoka, Suita, Osaka 565-0871 Japan*
[6]*University of Michigan, Ann Arbor, MI 48109*
[7]*Department of Physics, University of Oxford, Parks Road, OX1 3PU, United Kingdom*
[8]*LULI, Ecole Polytechnique, CNRS, Universit Paris 6, 91128 Palaiseau, France*
[9]*Princeton University, Princeton, NJ 08544*
[10]*Massachusetts Institute of Technology, Cambridge, Massachusetts 02139, USA*
[11]*Los Alamos National Laboratory, Los Alamos, New Mexico 87545, USA*

A study of the transition from collisional to collisionless plasma flows has been carried out at the National Ignition Facility (NIF) using high Mach number (M > 4) counterstreaming plasmas. In these experiments, CD-CD and CD-CH planar foils separated by 6 - 10 mm are irradiated with laser energies of 250 kJ per foil, generating ∼1000 km/s plasma flows. Varying the foil separation distance scales the ion density and average bulk velocity and therefore the ion-ion Coulomb mean free path, at the interaction region at the midplane. The characteristics of the flow interaction have been inferred from the neutrons and protons generated by deuteron-deuteron interactions and by x-ray emission from the hot, interpenetrating, and interacting plasmas. A localized burst of neutrons and bright x-ray emission near the mid-point of the counter-streaming flows was observed, suggesting strong heating and the initial stages of shock formation. As the separation of the CD-CH foils increases we observe enhanced neutron production compared to particle-in-cell simulations that include Coulomb collisions, but do not include collective collisionless plasma instabilities. The observed plasma heating and enhanced neutron production is consistent with the initial stages of collisionless shock formation, mediated by the Weibel filamentation instability.

Shocks are ubiquitous in the universe, triggered by explosive events such as supernovae and gamma-ray bursts [1, 2], energetic inflows such as those in accreting compact objects (such as white dwarfs), or the outflows produced by Active Galactic Nuclei [3–5]. The shocks produced in these energetic astrophysical settings are generally collisionless, meaning the Coulomb ion-ion collision mean free path (mfp) ≫ the thickness of the shock front or the interaction region. These shocks are thought to be a source of magnetic field generation and amplification [6, 7], and particle acceleration to cosmic ray energies [8–12]. Unlike the majority of shocks produced in the laboratory, which result from hydrodynamic (collisional) stagnation, astrophysical shocks rely on collective plasma behavior and instabilities to produce strong fields that can impede interpenetration sufficiently to form a shock. High Mach number (M > 4) collisionless shocks mediated by electromagnetic Weibel instabilities have not yet been generated in the laboratory; such experiments would enable the study of collisionless shock microphysics, and their predicted role in magnetic field generation, amplification, and high energy particle acceleration.

With the advent of high energy, high power lasers, the study of high Mach number collisionless plasma interactions became possible in the laboratory [13–16], with a number of experiments observing non-Weibel mediated (electrostatic, etc.) collisionless shocks [17–20]. The key questions related to the formation of Weibel mediated collisionless shocks in a laboratory are: 1) what are the required plasma conditions to form a collisionless shock and 2) what are the shock signatures in terms of fields and particle distributions. It is also important to understand the plasma conditions at the transition from collisional to collisionless flows in a laser experiment, where the preponderance of experimental work has been done in dense collisional plasma settings. Modern particle-in-cell simulations indicate that Weibel-mediated collisionless shocks can be formed for interpenetration distances $> 200c/\omega_{pi}$ [21], where $\omega_{pi} = \left(4\pi n_i Z^2 e^2/m_i\right)^{1/2}$ is the ion plasma frequency and c is the speed of light, however this has not yet been demonstrated experimentally.

Previous experiments [22] at the Omega Laser facility have demonstrated the development of Weibel-type filamentation instabilities [23, 24] that both generate a

seed magnetic field and amplifies it significantly, a critical step to forming a shock without preexisting background magnetic field [25, 26]. The plasma flow conditions were characterized using Thomson scattering (TS) [27]. The measurements indicate that the ion-ion Coulomb collision mfp is much greater than the interaction scale length [$\lambda_{ii}/$(foil separation) ~ 100] indicating the flows are in the collisionless regime. Proton radiography of the interaction showed the presence of the filamentary structures near the midplane where the overlap of the two streams occurred. The radius of individual filaments was consistent with the predictions of the linear theory of Weibel instability and PIC simulations, as was the magnetic field strength of more than 100 kG inferred from the proton radiographs [22]. Similar proton radiography results have been independently observed in experiments at Omega by other groups [28].

The TS measurements [27] in the region where the filaments were detected, however, have not revealed the increase of the ion temperature expected for shock formation: the ion temperature increased only to ~ 1.5 keV, whereas the Hugoniot value would be ~ 10 keV; the density also corresponded to a simple overlap of the streams (i.e., a factor of 2 increase relative to an individual stream). Although the Weibel instability had developed, the interpenetration distances ($< 50\ c/\omega_{pi}$) and time duration of the flows were not sufficient for shock formation and ion heating, consistent with PIC simulations [22].

The characteristic time scale for an e-folding of the Weibel instability is $(\omega_{pi}v/c)^{-1}$, where v is the flow velocity. It is therefore desirable to perform experiments at higher plasma density (higher ω_{pi}) and higher velocity, such that this time is shorter. This would allow the instability to reach a more developed state, eventually leading to shock formation. This scaling motivated a dedicated set of experiments on the National Ignition Facility (NIF) [29] at Lawrence Livermore National Laboratory. The NIF has 30 times higher laser energy available (compared to Omega, for this experimental configuration), well-characterized neutron diagnostics with neutron time-of-flight measurements along multiple chords, the capability to image self-emitted protons from the interaction region, and a variety of time-integrating X-ray imaging diagnostics. Characteristic parameters are shown in Table I. For NIF experiments, the number of instability e-folding times Γt_{max} (where Γ is the maximum growth rate and t_{max} is the time of peak neutron production) is indeed very large, in the range of a few hundred, allowing the instability to reach a highly developed non-linear stage due primarily to the factor of 40 increase in density compared to Omega experiments. On the other hand, the collision times are shorter than the duration of the experiment, especially for the shorter distance between the foils, meaning that collisional effects may still have significant influence on the distribution functions. This creates a situation where collisionless and
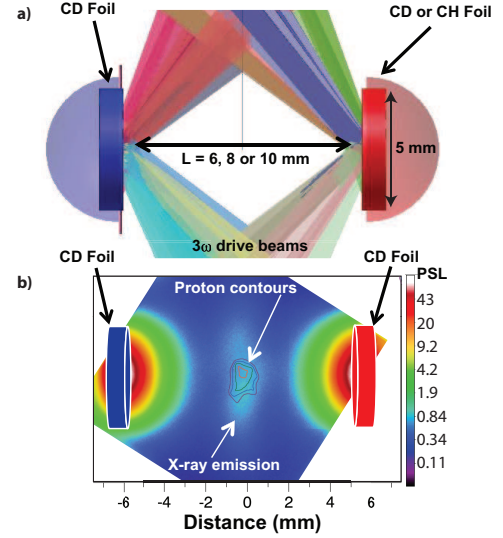

FIG. 1. (Color online) a) The experimental setup is shown for the double foil configuration. b) Measured single line of sight x-ray image and proton image contours are shown for the 10 mm separation target. The contour lines are 95, 90, 85 and 80% of the imaged self-generated proton yield.

collisional effects are tightly interwoven and both have to be accounted for.

In this Letter, we present the results from the first experiments on the initial stages of collisionless shock formation performed on the NIF. The experiments utilize solid density polystyrene foils (CH) and deuterated polystyrene foils (CD) that can generate 3 MeV protons and 2.45 MeV neutrons via nuclear reactions: $D(d,p)^3H$ and $D(d,n)^3He$. These reactions can originate from: 1) laser light directly heating the target foils; 2) beam-beam interactions for counter-streaming D ions; 3) small and large angle Coulomb scattering of D ions on the counter-propagating C ions; 4) scattering from random electromagnetic fields created by counterstreaming flow instabilities. A set of controlled experiments were performed to distinguish these individual components: single foil experiments to measure the effect of direct laser heating; CD-CH interpenetrating flows to see the contributions from stagnation heating and shock formation; and CD-CD to see the contribution of direct beam-beam interactions. From the counterstreaming CD-CD and CD-CH interpenetrating flows, the measured neutron and proton yields, spectrum, spatial distribution, and x-ray emissions allow us to characterize the interactions and differentiate the primary stagnation mechanisms. The measurements are compared to 2D particle-in-cell simulations of Coulomb ion scattering using the input from a 2D hydrodynamic simulation that modeled the laser/target interaction.

A typical experimental configuration is shown in Figure 1; a pair of CD-CD or CD-CH foils separated by 6 - 10 mm. The foils are each irradiated with forty-eight 351

TABLE I. Reference parameters for the Weibel instability and particle collisions. The plasma conditions are taken from the HYDRA and PIC simulations at the time of peak neutron production (t_{max}); n_e is the total electron density of the two overlapped streams, with the carbon and deuteron density per stream (for the CD-CD case) each being $n_e/14$. Case A: L=6 mm is the foil separation, t_{max}=5 ns; n_e=4×10^{20} cm^{-3}, v=1000 km/s; Case B: L=10 mm, t_{max}=9 ns; n_e=1.5×10^{20} cm^{-3}, v=1000 km/s; Definitions of the parameters are in the columns: (1) foil separation; (2) ion plasma frequency; (3) spatial scale of the Weibel filaments; (4) maximum (over the wave number) growth rate; (5) ion-ion collision mean free path length between the carbon ions of two interpenetrating streams; (6) the same for the deuterium ion of one stream and the carbon ions of the other; (7) collision time for the carbon ions. These parameters indicate that at 10 mm foil separation, the flow interactions are in a more collisionless regime.

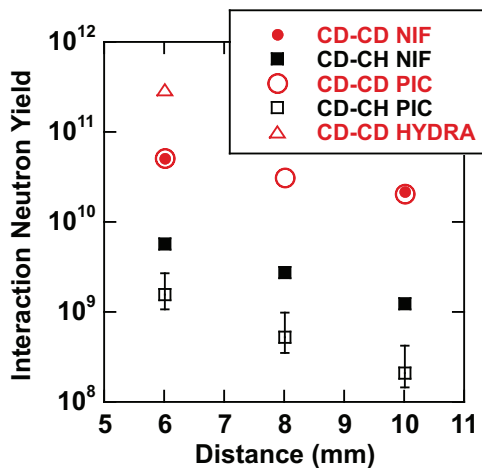|	1	2	3	4	5	6	7
	L, mm	ω_{pi}, ns^{-1}	$\pi c/\omega_{pi}$, μm	$\Gamma \equiv (v/c)\,\omega_{pi}$, ns^{-1}	λ_{CC}, mm	λ_{DC}, mm	$\tau_{CC} = \lambda_{CC}/v$, ns
A	6	2×10^4	50	70	4	10	4
B	10	1.2×10^4	85	40	11	27	11

FIG. 2. (Color online) The neutron yields from the interpenetrating plasma flow interactions are shown for the CD-CD foils (solid red circles) and the CD-CH foils (solid black squares). The measured single foil neutron yield of 4.7×10^8 is subtracted from the total measured yield (2x the single foil for CD-CD) to produce the plasma interaction yields. The uncertainty in the yield measurements is ±15% and less than the size of the data points. The simulated yield using HYDRA (open triangle) is shown for the 6 mm separation and the simulated yields using LSP are shown for CD foils (red open circles) and CD-CH foils (black open squares).

nm laser beams, each delivering 5.2 kJ in a 5 ns square pulse. The beams use continuous phase plates (CPPs) to produce focal spots with a supergaussian exponent of 4.3 and a full-width at half-maximum of 1200 μm resulting in an overlapped intensity of 2.8×10^{15} W/cm^2.

The self-generated protons and x-rays in the interpenetrating interaction region of the flows were imaged for each target configuration to determine the location of yield generation. The images were generated using a 1 mm diameter pinhole located 260 mm from the interaction, with CR39 positioned 1040 mm behind the pinholes backed with a Fuji BAS-SR image plate. The CR39 detects protons and is transparent to the x-rays which are in turn detected by the image plate. An example x-ray image overlaid with contours of the proton image is shown in Figure 1 b. Even though the x-ray image is dominated by emission near the foil surfaces where the plasma is directly laser heated, the central region where the two plasmas interact also shows considerable brightening in x-ray. A peak x-ray signal in the interaction region of 8.1 Photostimulated luminescence (PSL) for the 6 mm case, 2.1 PSL for the 8 mm case and 0.8 PSL for the 10 mm case is observed and is an indication of higher density and temperature in the 6 mm case. Strikingly, the proton emission region is completely dominated by the emission from the central region where the two plasma flows interact. This, in combination with the low single foil neutron yield, indicates the characteristics of neutron and proton measurements provide information about the interacting flows.

Neutron yield measurements integrated over time and angle are shown in Figure 2. A maximum yield of 5.3×10^{10} was observed for CD foils separated by 6 mm. A single foil CD shot showed a yield of 4.7×10^8, indicating the neutron yield for two foil experiments is dominated by the counter streaming plasma interaction. When one of the CD foils was replaced with CH, the yield dropped by a factor ∼8 to 6.3×10^9. A factor of 2 difference in yield between CD-CD and CD-CH is expected if a fully-formed strong shock is present, effectively isolating the deuterium to half the experimental volume in the CD-CH case. A factor of 8 yield reduction in the data indicates that the dominant contribution to the yield in the CD-CD case is beam-beam D interactions during interpenetration. However, the finite neutron generation in the CD-CH case indicates that there is either collisional or collisionless heating of the plasma. Without heating of the CD stream there would be no neutron generation as the counter-propagating stream has no deuterons for beam-beam generation. As this experimental case is at much higher density that previous Omega experiments, we cannot definitively conclude that all heating in the CD-CH case is collisionless. In fact, as shown in Table 1, the collisional mean-free-path is on the order of the system size. For this reason, we use collisional simula-
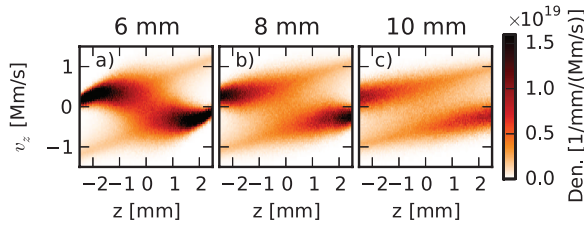
FIG. 3. (Color online) Simulated phase space diagrams (v_z vs z) of carbon for a) 6, b) 8 and c) 10 mm foil separations in the CD-CH cases at the time of peak neutron emission of 6.1, 7.5 and 9.3 ns, respectively. The transition from highly collisional (6 mm) to less collisional (10 mm) is evident by the limited number of particles near (0,0) in the third case.

tions to estimate the contribution of collisional processes to ion heating and neutron production.

Some level of ion-ion binary collisions is present due to the high densities achieved on the NIF and may contribute to the interaction between the streams. If Coulomb collisions were negligible in the CD-CH case, and collisionless plasma instabilities did not significantly affect the flows, the streams should have freely interpenetrated without producing any protons or neutrons. If collisions are present but weak, then the CD flow from one foil would be only slightly heated by the small-angle scattering off the carbon ions of the counter-propagating CH flow. As there are no deuterons in the counter-propagating stream, the intra-jet D-D collisions would be the only source of the neutrons and due to the minimal heating the total neutron yield would be negligible.

A 2D radiation hydrodynamics simulation using the code HYDRA [30] was completed for the 6 mm separation CD-CD foil experiment and found a neutron yield of 3×10^{11}, roughly a factor of 5 higher than that observed experimentally. The HYDRA simulation is a purely hydrodynamic collisional interaction of the two flows, in which two infinitesimally-thin shocks are formed and propagate away from the midpoint, with a shock heated neutron-generating plasma in between. This is an extreme case of the interaction between two highly-collisional flows. In our experiment, even the highest density flows corresponding to the 6 mm separation are not sufficiently collisional to be described as a fluid, which is a possible explanation of the difference between the neutron yield prediction from HYDRA and the observed results.

To properly take into account the finite collisional mean free path of our experiments, we have performed collisional simulations with the PIC code LSP [31]. The phase space diagrams from the LSP simulations are shown in Figure 3. For the 6 mm case the thermalization and neutron production time scales are predicted to be 1-2 ns, as expected when collisional interactions are significant. For the 10 mm foil separation, however, where collisional interactions are weaker, the thermaliza-

tion takes longer, of order ~10 ns. Note that the particle phase-space density is low near the z = 0, v_z = 0 region of the plot for the 10 mm separation but not for the 6 mm separation case. This again suggests that the 10 mm separation experiments are in a more collisionless regime, whereas the 6 mm separation experiments are rather collisional.

The simulations were initialized using the output of HYDRA runs at 3.5 ns from the start of the laser pulse. Given the uncertainty in the plasma conditions a series of simulations was completed where the electron density and flow velocity were varied to reproduce the 6 mm CD-CD neutron yield and spectrum. Synthetic neutron time-of-flight (ntof) data was generated from the simulations using the known detector responses. Thus simulated and experimental ntof data was compared directly and quantified via a reduced chi-squared significance test to all three ntof detectors at 5°, 97°, 139° from the CD target. While the neutron data is a time integrated diagnostic it highly constrains our simulations given that it constrains both the ion thermal velocity width (i.e. effective ion temperature) from the width of the neutron pulse, the flow velocity of the ions from the shift of the neutron pulse, and the ion density from the total yield. By matching the ntof data with our simulations of the 6 mm CD/CD case we constrained our simulations to agree to the 95% confidence level, which resulted in a constrained flow velocity of ±10% and ion density of ±25%. This set of simulations is used to generate uncertainties in the simulated neutron yield for the CD-CH cases shown in Fig. 2. The LSP simulations were run without any electro-magnetic fields, which assumes that the plasma expansion is ballistic. We used standard multiple, small-angle scattering (SAS) methods [32, 33] for all collisions with electrons. Due to the low collisionality of the plasma and the strong dependence of the neutron cross-section on velocity, we have included single, large angle scattering (LAS) events between and within ion species (e.g. D with D, D with C). The LAS algorithm is implemented in a similar way to that of Turrell *et al.* [34], but with a physically self-consistent transition between SAS and LAS.

The simulated neutron yields are compared to the experimental measurements in Figure 2. The simulated yield is that generated in the central interaction region which does not include the laser heated target surface region. The measured and LSP simulated yields for the 6 mm CD-CD case agree by construction. The spatial distribution of the proton emission is also similar (not shown). Reasonable agreement is observed for the neutron yield in the 10 mm case (Fig. 2). The dominant source of nuclear yield from the D-D reactions is from direct beam-beam binary collisions in the counter streaming CD-CD flows. As expected by both analytic calculations and simulations, in the CD-CH case, the absence of the counterstreaming deuterons leads to a large reduction

of the direct beam-beam yield by a factor of ~ 8 for 6 mm separation. The experimentally observed yield is larger than the simulated yield by a factor of ~ 6 for the CD-CH experiments. This suggests that there exists another source of scattering and reactions for the deuterons, other than Coulomb collisions; the strong electric and magnetic fields produced by streaming plasma instabilities appear a likely candidate. The discrepancy between the experimental results and collisional simulations increases with the target separation distance, consistent with the collisionless streaming plasma instabilities becoming more dominant (compared to binary ion-ion Coulomb collisions) at larger separations. At 10 mm foil separation, the average particle speed during the interactions near the mid-plane (z = 0) is higher and the density is lower, and thus collisionless collective plasma interactions are expected to be more important. Unfortunately, it is not possible to simulate both the full size of the experiment and include EM fields due to the computational expense in a PIC simulation. As done previously on Omega, it is possible to perform 3D simulations with EM fields, but only when using periodic boundary conditions to simulate a relatively small grid. However, such a periodic simulation will not be able to capture the 3D expansion of the target, which is necessary to obtain a quantitative neutron yield.

Given the earlier experimental results from Omega and the corresponding PIC simulations [22, 28], the collisionless interactions between the flows are expected to be driven by a Weibel-type instability [23, 24]. For the current NIF experimental conditions, this instability does not lead to a fully-developed collisionless shock. If it had, then the neutron yield for CD-CH would have been half of the CD-CD yield. The data does however clearly show enhanced ion scattering and localized electron heating, producing a local maximum in x-ray emission in the mid plane area. This is the region where the collisionless plasma instabilities are the strongest. These results suggest we are probing the nonlinear stage of the instability, which is mediating the initial stages of shock formation.

In conclusion, we have produced and characterized high velocity counter-streaming plasma flows relevant for the creation of collisionless shocks on the NIF. The interaction region has been characterized using a suite of particle and x-ray diagnostics and compared to 2D hydrodynamic and PIC simulations. We have found strong evidence for the presence of collective collisionless scattering of the particles in two interpenetrating flows. We have also observed that the relative importance of collisionless scattering compared to collisional scattering increases with increasing target separation: the interactions are significantly collisional at 6 mm separation, largely collisionless at 10 mm separation, and in transition at 8 mm separation. Combining our observations with those of earlier experiments on Omega, [22] we identify the most plausible candidate for the enhanced collisionless collective scattering and stagnation heating to be the filamentation Weibel instability.

[1] R. McCray and T. P. Snow, Jr, Annual Review of Astronomy and Astrophysics **17**, 213 (1979).

[2] C. P. McKee and D. J. Hollenbach, Annual Review of Astronomy and Astrophysics **18**, 219 (1980).

[3] M. C. Begelman, R. D. Blandford, and M. J. Rees, Reviews Of Modern Physics **56**, 255 (1984).

[4] E. M. de Gouveia Dal Pino, Advances in Space Research **35**, 908 (2005).

[5] A. Marcowith, A. Bret, A. Bykov, M. E. Dieckman, L. O. Drury, B. Lembege, M. Lemoine, G. Morlino, G. Murphy, G. Pelletier, I. Plotnikov, B. Reville, M. Riquelme, L. Sironi, and A. S. Novo, Reports On Progress In Physics **79**, 046901 (2016).

[6] R. A. Chevalier, Nature **266**, 701 (1977).

[7] G. Gregori, B. Reville, and F. Miniati, Physics Reports **601**, 1 (2015).

[8] S. A. Colgate and M. H. Johnson, Physical Review Letters **5**, 235 (1960).

[9] R. Blandford and D. Eichler, citeseerx.ist.psu.edu (1987).

[10] A. R. Bell, Monthly Notices of the Royal Astronomical Society **182**, 147 (1978).

[11] G. F. Krimsky, Dokl. Akad. Nauk SSSR **234** (1977).

[12] R. D. Blandford and J. P. Ostriker, The Astrophysical Journal Letters **221**, L29 (1978).

[13] R. P. Drake and G. Gregori, Astrophysical Journal **749**, 171 (2012).

[14] H.-S. Park *et al.*, High Energy Density Physics **8**, 38 (2012).

[15] D. D. Ryutov, N. L. Kugland, H. S. Park, C. Plechaty, B. A. Remington, and J. S. Ross, Plasma Physics And Controlled Fusion **54**, 105021 (2012).

[16] H. Ahmed, M. E. Dieckmann, L. Romagnani, D. Doria, G. Sarri, M. Cerchez, E. Ianni, I. Kourakis, A. L. Giesecke, M. Notley, R. Prasad, K. Quinn, O. Willi, and M. Borghesi, Physical Review Letters **110**, 205001 (2013).

[17] D. B. Schaeffer *et al.*, Physics of Plasmas **19**, 070702

(2012).

[18] C. Niemann *et al.*, Geophysical Research Letters **41**, 7413 (2014).

[19] L. Romagnani, S. V. Bulanov, M. Borghesi, P. Audebert, J. C. Gauthier, K. Loewenbrueck, A. J. Mackinnon, P. Patel, G. Pretzler, T. Toncian, and O. Willi, Physical Review Letters **101**, 025004 (2008).

[20] D. Haberberger, S. Tochitsky, F. Fiuza, C. Gong, R. A. Fonseca, L. O. Silva, W. B. Mori, and C. Joshi, Nature Physics **8**, 95 (2011).

[21] T. N. Kato and H. Takabe, Astrophysical Journal Letters **681**, L93 (2008).

[22] C. M. Huntington *et al.*, Nature Physics **11**, 173 (2015).

[23] E. Weibel, Physical Review Letters **2**, 83 (1959).

[24] B. D. Fried, Physics Of Fluids **2**, 337 (1959).

[25] A. Spitkovsky, The Astrophysical Journal **682**, L5 (2008).

[26] F. Fiuza, R. A. Fonseca, J. Tonge, W. B. Mori, and L. O. Silva, Physical Review Letters **108**, 235004 (2012).

[27] J. S. Ross *et al.*, Physics Of Plasmas **19**, 056501 (2012).

[28] W. Fox, G. Fiksel, A. Bhattacharjee, P. Y. Chang, K. Germaschewski, S. X. Hu, and P. M. Nilson, Physical Review Letters **111**, 225002 (2013).

[29] G. H. Miller, E. I. Moses, and C. R. Wuest, Optical Engineering **43**, 2841 (2004).

[30] M. M. Marinak, G. D. Kerbel, N. A. Gentile, O. Jones, D. Munro, S. Pollaine, T. R. Dittrich, and S. W. Haan, Physics Of Plasmas **8**, 2275 (2001).

[31] D. R. Welch, D. V. Rose, R. E. Clark, T. C. Genoni, and T. P. Hughes, Computer Physics Communications **164**, 183 (2004).

[32] T. Takizuka and H. Abe, Journal of Computational Physics **25**, 205 (1977).

[33] K. Nanbu, Physical Review E **55**, 4642 (1997).

[34] A. E. Turrell, M. Sherlock, and S. J. Rose, Journal of Computational Physics **299**, 144 (2015).